Philosophical Magazine

ISSN: (Print) (Online) Journal homepage: https://www.tandfonline.com/loi/tphm20

Measuring the imaginary-time dynamics of quantum materials

S. Lederer , D. Jost , T. Böhm , R. Hackl , E. Berg & S. A. Kivelson

To cite this article: S. Lederer , D. Jost , T. Böhm , R. Hackl , E. Berg & S. A. Kivelson (2020) Measuring the imaginary-time dynamics of quantum materials, Philosophical Magazine, 100:19, 2477-2490, DOI: 10.1080/14786435.2020.1768604

To link to this article: https://doi.org/10.1080/14786435.2020.1768604

Published online: 28 May 2020.

PHILOSOPHICAL MAGAZINE
2020, VOL. 100, NO. 19, 2477–2490
https://doi.org/10.1080/14786435.2020.1768604

Taylor & Francis
Taylor & Francis Group

Measuring the imaginary-time dynamics of quantum materials

S. Lederer[a], D. Jost [b,c], T. Böhm[b,c*], R. Hackl[b], E. Berg[d] and S. A. Kivelson[e]

[a]Department of Physics, Cornell University, Ithaca, NY, USA; [b]Walther Meissner Institut, Bayerische Akademie der Wissenschaften, Garching, Germany; [c]Fakultät für Physik E23, Technische Universität München, Garching, Germany; [d]Department of Condensed Matter Physics, The Weizmann Institute of Science, Rehovot, Israel; [e]Department of Physics, Stanford University, Stanford, CA, USA

ABSTRACT

Theoretical analysis typically involves imaginary-time correlation functions. Inferring real-time dynamical response functions from this information is notoriously difficult. However, as we articulate here, it is straightforward to compute imaginary-time correlators from the *measured* frequency dependence of (real-time) response functions. In addition to facilitating comparison between theory and experiment, the proposed approach can be useful in extracting certain aspects of the (long-time relaxational) dynamics from a complex data set. We illustrate this with an analysis of the nematic response inferred from Raman scattering spectroscopy on the iron-based superconductor $Ba(Fe_{1-x}Co_x)_2As_2$, which includes a new method for identifying a putative quantum-critical contribution to that response.

ARTICLE HISTORY
Received 1 April 2020
Accepted 6 May 2020

KEYWORDS
Quantum critical phenomena; spectroscopy; strongly correlated electrons

Spectroscopic probes provide a wealth of information about the dynamics of quantum systems. Spectra are often very complicated. Sometimes, however, individual spectral features are of less interest than the overall evolution of the spectrum as parameters (such as temperature, pressure, doping, or magnetic field), are varied. In this setting, it is necessary to condense the considerable information in each spectrum into a few numbers. We propose a new method for doing this based on the computation of correlation functions in the *imaginary* time domain. The method is unbiased, numerically reliable and allows unambiguous comparison with the results of state of the art numerical methods.

It goes without saying that laboratory experiments measure real-time correlators. However, many theoretical methods that have been deployed to extract non-perturbative results on strongly interacting quantum systems, including various forms of quantum Monte Carlo studies, work exclusively in imaginary

CONTACT S. Lederer samuel.lederer@gmail.com Department of Physics, Cornell University, Ithaca, NY, USA; D. Jost daniel.jost@wmi.badw.de Walther Meissner Institut, Bayerische Akademie der Wissenschaften, 85748 Garching, Germany
*Present address: TNG Technology Consulting GmbH, Beta-Strasse, 85774 Unterföhring, Germany

time. Given the uncertainties in analytic continuation, one reason to compute imaginary-time correlators from laboratory data is that it transforms it into a form that can be directly compared with this class of theoretical results.

The transformation from real frequency to imaginary time, discussed in further detail below, discards much of the rich information present in real-time data. For instance, a well defined normal mode (quasiparticle) with an energy $\epsilon \gg k_B T$ (with T the temperature) shows up as a sharp peak in an appropriate real frequency response function, but the corresponding feature in the imaginary-time correlator varies as $\exp[-\epsilon\tau/\hbar]$, and so makes no contribution to long-time properties. On the other hand, the long-time relaxational dynamics of a system – the dynamics that control its approach to equilibrium – typically dominate the long-imaginary-time dynamics as well. Thus, using measured response functions to compute long-imaginary-time behaviour of the corresponding correlators can be viewed as a method of intrinsic and unbiased filtering, which extracts certain interesting information from a complex spectral response.

In principle, it is possible to compute the real-time (or frequency, ω) fluctuational dynamics of any system in equilibrium from imaginary-time (or Matsubara frequency, ω_n) correlation functions and vice versa. In practice, inferring real-time dynamics from imaginary-time data involves an analytic continuation that can rarely be carried out without additional assumptions. This ambiguity follows from the fact that the discrete Matsubara frequencies, ω_n, have spacing $\Delta\omega \equiv \omega_{n+1} - \omega_n = 2\pi k_B T/\hbar$, making features which vary as a function of ω more rapidly than $\Delta\omega$ difficult to discern in the imaginary-time response functions. It is, however, straightforward to compute imaginary-time correlation functions from measured real frequency quantities.

Here, we give explicit formulas for computing imaginary-time correlators from response functions measurable in the laboratory. Building on the work in Ref. [1–3], we treat explicitly the general case of linear response of (bosonic) physical observables, as well as the electron spectral function (measurable in tunnelling and photo-emission spectroscopy). To illustrate what information is emphasised and what is suppressed, we carry out this programme for various simple and physically plausible assumed forms of a response function. Finally, to illustrate the usefulness of the approach, we take high resolution Raman data measured on $Ba(Fe_{1-x}Co_x)_2As_2$ in the B_{2g} channel[4] and compute the corresponding imaginary-time correlator, which yields a sharp diagnostic of the structural transition in that channel.

1. Computing imaginary-time correlators from spectroscopic measurements

1.1. Dissipative linear-response functions

For any observables Φ_a and Φ_b, it follows from linear-response theory and the fluctuation dissipation theorem that there is a relation between the dissipative

part of the linear response function, $\chi''_{ab}(\omega)$, and the imaginary-time-ordered correlation function, $\tilde{\Lambda}_{ab}(\tau)$:

$$\tilde{\Lambda}_{ab}(\tau) = \int \frac{d\omega}{2\pi}\ \chi''_{ab}(\omega)\ \left[\frac{\exp(\omega[\tau - \beta/2])}{\sinh(\beta\omega/2)}\right], \tag{1}$$

where (in units in which $k_B = \hbar = 1$) χ'' is the Fourier transform of

$$\tilde{\chi}''_{ab}(t) \equiv \frac{1}{2}\langle[\Phi_a(t), \Phi_b(0)]\rangle, \tag{2}$$

and, for $0 \leq \tau \leq \beta$

$$\tilde{\Lambda}_{ab}(\tau) \equiv \langle\Phi_a(-i\tau)\Phi_b(0)\rangle, \tag{3}$$

with $\beta = 1/T$. The relation between χ'' and the imaginary-time correlation function in the Matsubara frequency domain is

$$\Lambda_{ab}(\omega_n) = \int \frac{d\omega}{\pi}\ \chi''_{ab}(\omega)\ \left[\frac{\omega}{\omega^2 + \omega_n^2}\right], \tag{4}$$

where $\omega_n = 2\pi nT$. Because $\tilde{\Lambda}_{ab}(\tau)$ is a bosonic correlator, $\tilde{\Lambda}_{ab}(\tau) = \tilde{\Lambda}_{ba}(\beta - \tau)$. Thus, if we are interested in the 'long-time' behaviour of $\tilde{\Lambda}_{ab}$, we mean we are interested in the longest-possible times, *i.e.* $\tau \approx \beta/2$. The important point to note about Equation (1) is that for $\tau \approx \beta/2$, the integral is dominated by the range of frequencies $|\omega| \lesssim T$, so *the long-imaginary time dynamics can be computed from measurements of the response function in a very limited range of frequencies.*

As one important example, let Φ_a be a component of the electrical current operator, whose associated susceptibility is proportional to the conductivity. Let $\sigma'_{aa}(\omega)$ be the real part of the optical conductivity, and $\tilde{\Lambda}_{aa}(\tau)$ be the imaginary-time ordered current-current correlator. Here a is a tensor index indicating a spatial direction. The Kubo formula relates the conductivity to χ'', and consequently[3]

$$\tilde{\Lambda}_{aa}(\tau) = \int \frac{d\omega}{2\pi}\ \omega\sigma'_{aa}(\omega)\ \left[\frac{\cosh[\omega(\beta/2 - \tau)]}{\sinh(\beta\omega/2)}\right]. \tag{5}$$

The other case we treat here is where Φ_a is an order parameter field. For instance, Φ_a could be a component of the spin density at an appropriate ordering vector $\vec{Q}$, so that the resulting susceptibility (which has a singular response near a magnetic transition) can be measured in inelastic neutron scattering. If Φ_a is a component of the fermion quadrupole density in some symmetry channel (B_{1g}, B_{2g}, etc.), then the resulting susceptibility (which has a singular response near a nematic transition), can be measured in non-resonant Raman scattering[5].

1.2. Electronic spectral function

Similar expressions relate the imaginary-time-ordered Green function, $\tilde{G}(\vec{k}, \tau)$ to the single particle spectral function, $A(\vec{k}, \omega) \equiv -1/\pi Im(\mathcal{G}(\vec{k}, \omega))$, where $\mathcal{G}$ is the real frequency (retarded) Green function[2].

$$\begin{aligned}\tilde{G}(\vec{k}, \tau) &= \int d\omega\, A(\vec{k}, \omega) \left[\frac{\exp[\omega(\beta/2 - \tau)]}{2\cosh(\beta\omega/2)}\right], \\ &= \int d\omega\, I(\vec{k}, \omega)\ \exp[\omega(\beta - \tau)],\end{aligned} \tag{6}$$

where $\vec{k}$ is the momentum (or Bloch wave-vector), we have assumed τ in the range $0 \leq \tau < \beta$, and $I(\vec{k}, \omega) \equiv f(\omega)A(\vec{k}, \omega)$ is the occupation-weighted spectral function (as measured in ARPES), where $f(\omega) = [e^{\beta\omega} + 1]^{-1}$ is the Fermi function. Again, except at very short imaginary times, the imaginary-time correlator can be readily computed from the experimentally measured response function over a range of frequencies of order T about the Fermi energy.

In Appendix 1 we explicitly derive the transformations for a few special cases relevant for correlated systems including the marginal Fermi liquid[6] and power-law scaling close to a quantum-critical point.

2. The imaginary-time quadrapolar correlations in $Ba(Fe_{1-x}Co_x)_2As_2$

Here we apply the proposed analysis to the experimentally measured temperature (T) and doping (x) dependent Raman response of $Ba(Fe_{1-x}Co_x)_2As_2$, with particular focus on the critical electronic quadrapolar fluctuations in the vicinity of the structural (nematic) transition at T_s.

2.1. The static susceptibility and $\tilde{\Lambda}(\beta/2)$

Raman scattering measures a dissipative response, and can therefore yield the imaginary part $\chi''(\omega, T)$ of an appropriate susceptibility. The static value of the real part of the susceptibility, $\chi'(0, T)$, is related to $\chi''(\omega, T)$ by the Kramers–Kronig transformation,

$$\chi'(0, T) = \int \frac{d\omega}{\pi} \frac{\chi''(\omega, T)}{\omega}. \tag{7}$$

Note that Equation (4) reduces to Equation (7) when $\omega_n = 0$, so that $\Lambda(0) = \chi'(0, T)$. In practice, $\chi'(0, T)$ can almost never be precisely determined from Raman measurements, because the integrand falls off too weakly at large frequency, necessitating an arbitrary cut-off procedure; this is a generic problem with Kramers–Kronig analysis. As an alternative, one can use the same data to determine the value of the imaginary-time correlator at time

$\beta/2$, via

$$\tilde{\Lambda}(\beta/2) = \int \frac{d\omega}{2\pi} \frac{\chi''(\omega)}{\sinh(\beta\omega/2)}. \tag{8}$$

Since $|\sinh(x)| \geq |x|$ for all x (with the inequality saturated as $x \to 0$), we have the following inequality,

$$\tilde{\Lambda}(\beta/2) \leq T \int \frac{d\omega}{\pi} \frac{\chi''(\omega)}{\omega} = T\chi'(0). \tag{9}$$

Evidently $\tilde{\Lambda}(\beta/2)/T$ is bounded above by the static susceptibility, with the bound nearly saturated when spectral weight is concentrated at frequencies $\omega \ll T$. In fact, $\tilde{\Lambda}(\beta/2)/T$ contains the same universal information as the static susceptibility under a wide range of assumptions. For instance, at a continuous phase transition at nonzero temperature, $\tilde{\Lambda}(\beta/2)/T$ has the same divergent behaviour as the static susceptibility. This can be seen by writing the quantity in Fourier transform:

$$\begin{aligned} \tilde{\Lambda}(\beta/2) &= T \sum_n e^{-i\nu_n \beta/2} \Lambda(\nu_n) \\ &= T \sum_n (-1)^n \Lambda(\nu_n) \\ &= T\chi'(0, T) + \ldots, \end{aligned} \tag{10}$$

where we have used the fact that $\Lambda(0) = \chi'(0, T)$, and dots refer to the contribution from nonzero Matsubara frequencies which, per Equation (4), are insensitive to the asymptotically low frequencies at which critical behaviour in χ'' is found. At a quantum-critical point obeying ω/T scaling, $\tilde{\Lambda}(\beta/2)/T$ also has the same divergence as the static susceptibility in the low temperature limit.

A key practical advantage of $\tilde{\Lambda}(\beta/2)/T$ as a measure of low frequency fluctuations is the fact that the $\sinh(\beta\omega/2)$ in the denominator of Equation (10) yields an exponential cut-off at high energies the scale of which is given by temperature. This means that $\tilde{\Lambda}(\beta/2)/T$, unlike $\chi'(0)$, is subject to essentially no error due to a lack of knowledge of high frequencies. As we will show, it is therefore a valuable and unambiguous method of analysis for Raman spectra.

2.2. Raman spectra of Co-doped $BaFe_2As_2$

We demonstrate now the effect of using the dimensionless imaginary-time correlation function $\beta\tilde{\Lambda}(\beta/2, T)$ for the analysis of Raman spectra and put it into perspective with other methods for extracting properties in the low frequency limit. In particular, we compare the results obtained for $\beta\tilde{\Lambda}(\beta/2, T)$ with the static Raman susceptibility $\chi'(0, T)$.

To this end we have extended earlier measurements[7, 8] of the Raman spectra of $Ba(Fe_{1-x}Co_x)_2As_2$ both to obtain data over a wider range of energies, and to access a finer grid of temperatures. By extending the range of frequencies up to 1000 cm^{-1} we ensure that the range is sufficient to unambiguously determine $\beta\tilde{\Lambda}(\beta/2, T)$ even at room temperature, where 1000 cm^{-1} is 4.7 k_BT. The dense average grid of temperatures, $\bar{\Delta T} = 23$ K, is needed to identify critical behaviour in the neighbourhood of the structural transition temperature, T_s.

Figure 1 shows the Raman spectra of overdoped $Ba(Fe_{0.915}Co_{0.085})_2As_2$ in the $A_{1g} + A_{2g}$ channel [essentially s-wave, panel (a)] and the $B_{2g} + A_{2g}$ [d-wave-like, panel (b)]. The spectra are constant and temperature independent (to within $\pm 5\%$) at energies above 700 cm^{-1}. Below 700 cm^{-1} the intensity increases upon cooling, with the $B_{2g} + A_{2g}$ spectra (Figure 1 (b)) displaying a slightly stronger variation. Figure 2 shows the same data, but now presented as a function of scaled variables. Sufficiently close to certain quantum-critical points, one expects critical response functions to exihibit ω/T scaling, which would mean that scaling the data at various T and ω as in the figure would collapse the data onto a single curve. The data in the B_{2g} channel shows an approximate version of such a scaling collapse; the A_{1g} data somewhat less so.

Figure 3 shows $\beta\tilde{\Lambda}(\beta/2, T)$ and $\chi'(0, T)$ extracted from the B_{2g} Raman data of $Ba(Fe_{1-x}Co_x)_2As_2$ using Eqs. (7,8) for a range of doping concentrations, x

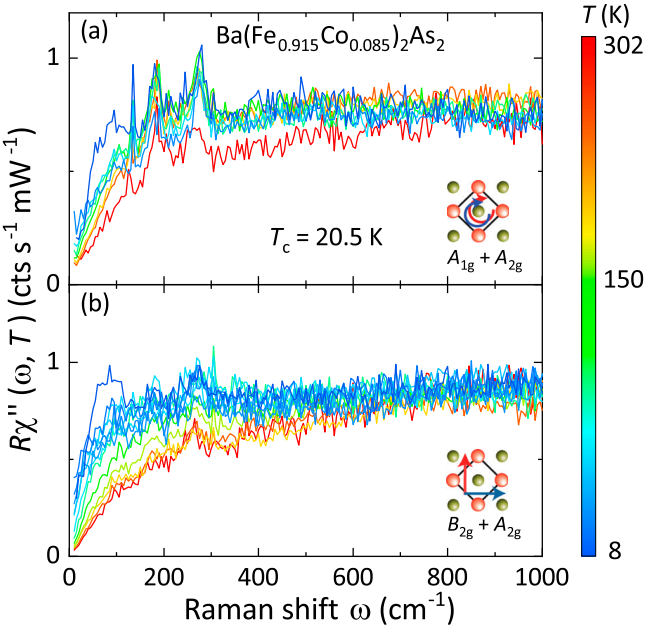

Figure 1. Raw data of the Raman response $R\chi''(\Omega, T)$ of $Ba(Fe_{0.915}Co_{0.085})_2As_2$. We use a continuous colour scale for the temperature (right scale bar). The (a) $A_{1g} + A_{2g}$ and (b) $B_{2g} + A_{2g}$ spectra are measured in RR ($R = (x + iy)/\sqrt{2}$) and xy polarisation, respectively, where x and y are the axes of the 2 Fe crystallographic cell in the tetragonal phase as indicated pictorially.

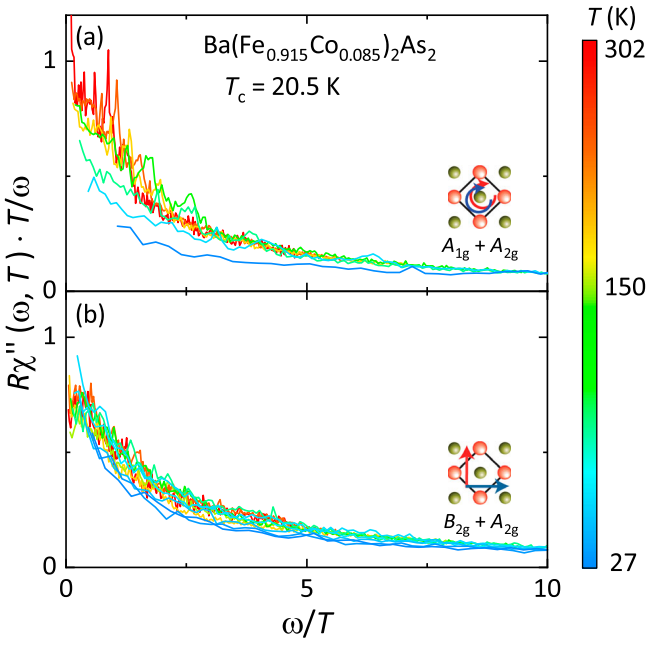

Figure 2. Same data as in Figure 1, but now in terms of scaled variables. The y axis is $\chi''(\omega, T) \cdot T/\omega$ and the x axis is ω/T. Only data for $T > T_c = 20.5$ K is shown.

below ($x \leq 0.051$) and above (x=0.085) a putative quantum-critical point at $x_c \approx 0.06$. The scale on the left and right ordinates (for $\beta\tilde{\Lambda}(\beta/2, T)$ and $\chi'(0, T)$ respectively) are chosen so that the two curves coincide at high T. For x<0.085 the two quantities show a qualitatively similar temperature dependence above the structural transition temperature, at which they both have a cusp singularity. However, as x increases, the temperature dependence of $\beta\tilde{\Lambda}(\beta/2, T)$ weakens much more rapidly than that of $\chi'(0, T)$. The two measures show meaningfully distinct behaviour at x=0.085, where $\chi'(0, T)$ increases by nearly a factor of two upon cooling to 50 K, while $\beta\tilde{\Lambda}(\beta/2, T)$ remains constant.

It is important to stress that there is an unavoidable uncertainty in the inferred values of χ'. Specifically, since $\chi''(\omega, T)$ is essentially constant at high energies (see Figure 1), to compute $\chi'(0, T)$ one must cut-off the Kramers–Kronig integral, in which case the result depends logarithmically on the cut-off. A corollary of this is that the degree of temperature dependence of χ' depends strongly on the cut-off. In contrast, the weighting factor $[\sinh(\beta\omega/2)]^{-1}$ in Equation (8) decays exponentially, making the integral unique so long as the spectra are measured up to energies of a few times the temperature. In any case, as anticipated above, $\chi'(0, T)$ and $\beta\tilde{\Lambda}(\beta/2, T)$ have near-identical singularities at the structural transition temperature T_s in underdoped $Ba(Fe_{1-x}Co_x)_2As_2$ with $x \lesssim 0.06$. The lack of a genuine divergence at the transition is likely an effect of electron-phonon coupling[9].

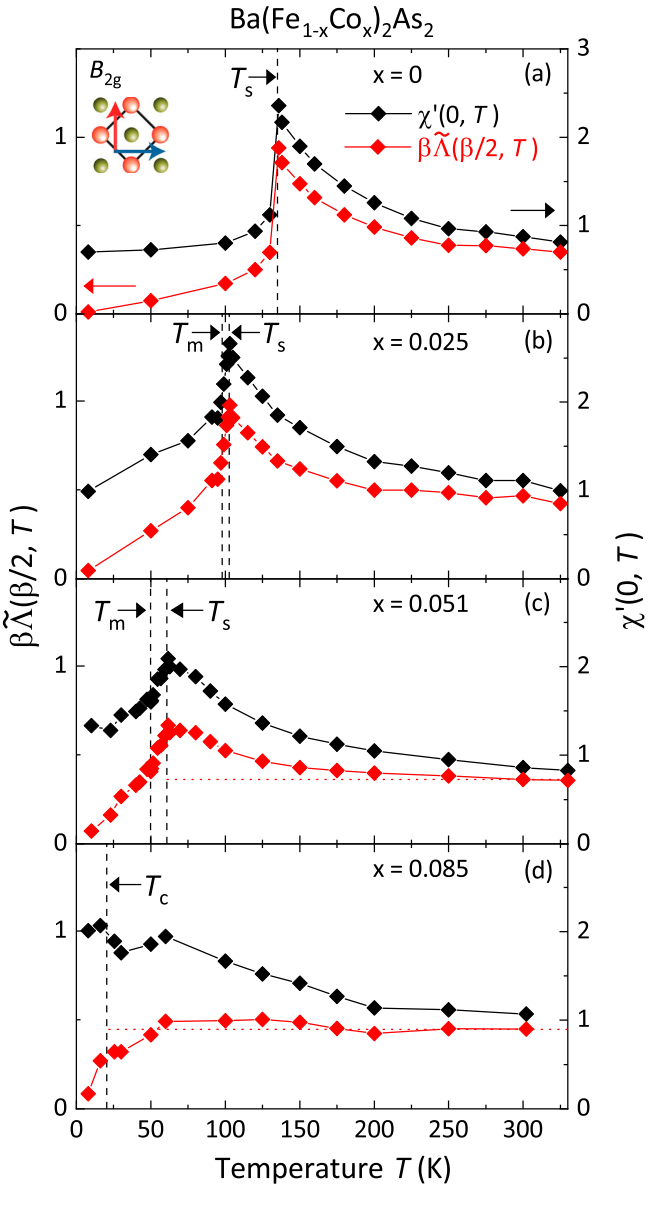

Figure 3. Temperature dependence of two different measures of the low frequency Raman response of $Ba(Fe_{1-x}Co_x)_2As_2$ in the B_{2g} symmetry channel. The doping concentration x determines the distance from a putative QCP at $x_c \approx 0.06$ between 0.051 and 0.085. T_s, T_m and T_c are the structural, magnetic and superconducting transition temperatures, respectively. At x=0 T_s and T_m coincide. Shown in black (right axis) is the static susceptibility $\chi'(0, T)$, computed from the measured $\chi''(\omega, T)$ using the Kramers–Kronig relation of Equation (7), integrated up to a cut-off frequency of 1000 cm^{-1} (approximately 124 meV). In red (left axis) is the suitably scaled imaginary-time correlation function $\tilde{\Lambda}(\beta/2, T)$, defined in Equation (8). Both quantities capture the singular temperature dependence of the Raman response near the structural transition, but the imaginary-time correlator requires no manual cut-off procedure. The two quantities differ most substantially near zero temperature, where $\tilde{\Lambda}(\beta/2, T)$ must vanish, since it only captures the dynamics at frequencies of order the temperature. The Raman data for $x \leq 0.051$ are published in Ref. [8], while those with $x = 0.085$ are shown in Figure 1.

3. Discussion

In this paper, we discuss a method to analyse experimental spectroscopic data by transforming it to imaginary time. This method is applicable to almost any experimental probe which measures response functions at frequencies of order the temperature (for additional examples see Appendix 1). In particular, the appropriate response function at maximal imaginary time separation, $\beta\tilde{\Lambda}(\beta/2)$, can be computed without an arbitrary cut-off procedure, and is a quantitative measure of low frequency spectral weight. For the optical conductivity, $\beta\tilde{\Lambda}(\beta/2)$ is a physically motivated definition of a low frequency 'Drude weight'.[10] In inelastic neutron scattering, a drop in $\beta\tilde{\Lambda}(\beta/2)$ as a function of temperature can quantify the development of a spin gap. In angle resolved photo-emission spectroscopy, $\beta\tilde{\Lambda}(\beta/2)$ is a proxy for the quasiparticle residue Z. [11] The experimental measurement of imaginary-time response functions is a potentially powerful tool both for the quantification of low frequency spectral properties, and for bridging experiment and theory.

Framing the analysis in terms of $\beta\tilde{\Lambda}(\beta/2, T)$ has three advantages: (i) This quantity can be computed directly and unambiguously from the measured χ''; (ii) it can be directly compared with theoretical predictions performed in the imaginary-time domain [11]; (iii) it highlights asymptotic low-energy physics by suppressing the effects of high energy spectral features.

This last point is vividly illustrated by considering the Raman data in Figure 3 (d) ($Ba(Fe_{1-x}Co_x)_2As_2$ with x=0.085). A constant value of $\beta\tilde{\Lambda}(\beta/2, T)$ indicates that χ'' exhibits ω/T scaling in a range of frequencies that extends to well above $\omega = T$. Such scaling up to a microscopic cut-off scale, Ω, is a hallmark of the 'marginal Fermi liquid' phenomenology (see Sec. A.3). In this case, $\chi'(0, T)$ would be expected to have a weak (logarithmic) T dependence, while deviations of $\beta\tilde{\Lambda}(\beta/2, T)$ from a constant value would be small for $T \ll \Omega$. Accordingly, the temperature dependence of $\beta\tilde{\Lambda}(\beta/2, T)$ suggests an intermediate asymptotic range of singular behaviour in χ'' in a range of frequencies and temperatures $T_c \ll \omega, T \ll \Omega$, while the temperature dependence of $\chi'(0, T)$ does not clearly manifest such behaviour. (The extent to which the indicated scaling is actually obeyed is exhibited in Figure 2). Thus, the imaginary-time analysis is particularly suited to reveal the emergent ω/T scaling behaviour at low frequencies.

Indeed, there is abundant evidence[7, 12–16] for nematic fluctuations near a putative quantum-critical point (QCP) in $Ba(Fe_{1-x}Co_x)_2As_2$ at $x = x_c \approx 0.06$. This would imply the existence of a quantum-critical fan in the x–T plane that is bounded by crossover lines, $T^*(x) \sim |x - x_c|^y$ (where y is an appropriate critical exponent). While these considerations are only precise asymptotically close to the putative QCP, suggestive evidence of the existence of such a crossover scale is apparent in Figure 3. In particular, $\beta\tilde{\Lambda}(\beta/2, T)$ for x=0.085 is

approximately constant in the B_{2g} channel (as indicated by the dotted line in the figure) until it deviates downward below $T^* \approx 60$ K, while for x=0.051 it rises (as 'classical' critical fluctuations associated with the approach to the ordered phase become significant) below $T^* \sim 150$ K. This, we feel, is a clear example of a way in which the present mode of analysis can lead to new ways to interpret data; whether what is at play is truly quantum critical nematic fluctuations can be tested by obtaining data closer to criticality, both by studying samples with x closer to x_c and, by suppressing superconductivity with a magnetic field, following the behaviour to lower T.

Acknowledgments

We acknowledge helpful discussions with A. Baum, M. Randeria, R. Scalettar and N. Trivedi. D. J. and R. H. gratefully acknowledge the hospitality of the the Stanford Institute for Materials and Energy Sciences (SIMES) at Stanford University and SLAC National Accelerator Laboratory. Financial support for the work came, in part, from the Friedrich-Ebert-Stiftung (D.J.), the Deutsche Forschungsgemeinschaft (DFG) via the Priority Program SPP 1458 (D. J., T. B. and R. H. project no. HA 2071/7-2), the Collaborative Research Center TRR 80 (D. J. and R. H., Project ID 107745057), and the Bavaria California Technology Center BaCaTeC (S. A. K., D. J. and R. H., project no. 21[2016-2]). S. A. K. was supported in part by NSF grant # DMR-1608055 at Stanford, S. L. was supported by a Bethe/KIC fellowship at Cornell, and E. B. was supported by the European Research Council under grant HQMAT (#817799) and by the Minerva foundation.

Disclosure statement

No potential conflict of interest was reported by the author(s).

Funding

We acknowledge helpful discussions with A. Baum, M. Randeria, R. Scalettar and N. Trivedi. D.J. and R.H. gratefully acknowledge the hospitality of the the Stanford Institute for Materials and Energy Sciences (SIMES) at Stanford University and SLAC National Accelerator Laboratory. Financial support for the work came, in part, from the Friedrich-Ebert-Stiftung (D.J.), the Deutsche Forschungsgemeinschaft (DFG) via the Priority Program SPP 1458 (D.J., T.B. and R.H. project no. HA 2071/7-2), the Collaborative Research Center TRR80 (D.J. and R.H., Project ID 107745057) and the Bavaria California Technology Center BaCaTeC (S.A.K., D.J. and R.H., project no. 21[2016-2]). S.A.K. was supported in part by NSF grant # DMR-1608055 at Stanford, S.L. was supported by a Bethe/KIC fellowship at Cornell and E.B. was supported by the European Research Council under grant HQMAT (#817799) and by the Minerva foundation.

ORCID

D. Jost http://orcid.org/0000-0001-7327-7789

References

[1] M. Randeria, N. Trivedi, A. Moreo, and R.T. Scalettar, *Pairing and spin gap in the normal state of short coherence length superconductors*, Phys. Rev. Lett. 69 (1992), pp. 2001–2004. doi:10.1103/PhysRevLett.69.2001

[2] N. Trivedi and M. Randeria, *Deviations from Fermi-liquid behavior above T_c in 2D short coherence length superconductors*, Phys. Rev. Lett. 75 (1995), pp. 312–315. doi:10.1103/PhysRevLett.75.312

[3] N. Trivedi, R.T. Scalettar, and M. Randeria, *Superconductor-insulator transition in a disordered electronic system*, Phys. Rev. B 54 (1996), pp. R3756–R3759. doi:10.1103/PhysRevB.54.R3756

[4] We use the crystallographic two-iron unit cell. In the one-iron unit cell this would be B_1g.

[5] B.S. Shastry and B.I. Shraiman, *Theory of Raman scattering in Mott-Hubbard systems*, Phys. Rev. Lett. 65 (1990), pp. 1068–1071. doi:10.1103/PhysRevLett.65.1068

[6] C.M. Varma, P.B. Littlewood, S. Schmitt-Rink, E. Abrahams, and A.E. Ruckenstein, *Phenomenology of the normal state of Cu-O high-temperature superconductors*, Phys. Rev. Lett. 63 (1989), pp. 1996–1999. doi:10.1103/PhysRevLett.63.1996

[7] Y. Gallais, R.M. Fernandes, I. Paul, L. Chauvière, Y.-X. Yang, M.-A. Méasson, M. Cazayous, A. Sacuto, D. Colson, and A. Forget, *Observation of incipient charge nematicity in* $Ba(Fe_1-XCo_X)_2As_2$, Phys. Rev. Lett. 111 (2013), pp. 267001. doi:10.1103/PhysRevLett.111.267001

[8] F. Kretzschmar, T. Böhm, U. Karahasanović, B. Muschler, A. Baum, D. Jost, J. Schmalian, S. Caprara, M. Grilli, C. Di Castro, J.H. Analytis, J.-H. Chu, I.R. Fisher, and R. Hackl, *Critical spin fluctuations and the origin of nematic order in* $Ba(Fe_1 - xCo_x)_2As_2$, Nat. Phys. 12 (2016), pp. 560–563. doi:10.1038/NPHYS3634

[9] Y. Gallais and I. Paul, *Charge nematicity and electronic Raman scattering in iron-based superconductors*, C. R. Phys. 17 (2016), pp. 113–139. iron-based superconductors / Supraconducteurs base de fer doi:10.1016/j.crhy.2015.10.001

[10] S. Lederer, Y. Schattner, E. Berg, and S.A. Kivelson, *Superconductivity and non-Fermi liquid behavior near a nematic quantum critical point*, PNAS 114 (2017), pp. 4905–4910. doi:10.1073/pnas.1620651114

[11] Y. Schattner, S. Lederer, S.A. Kivelson, and E. Berg, *Ising nematic quantum critical point in a metal: A Monte Carlo study*, Phys. Rev. X 6 (2016), pp. 031028. doi:10.1103/PhysRevX.6.031028

[12] J.-H. Chu, H.-H. Kuo, J. G. Analytis, and I. R. Fisher, *Divergent nematic susceptibility in an iron arsenide superconductor*, Science 337 (2012), pp. 710–712. doi:10.1126/science.1221713

[13] A.E. Böhmer, P. Burger, F. Hardy, T. Wolf, P. Schweiss, R. Fromknecht, M. Reinecker, W. Schranz, and C. Meingast, *Nematic susceptibility of hole-doped and electron-doped* $BaFe_2As_2$ *iron-Based superconductors from shear modulus measurements*, Phys. Rev. Lett. 112 (2014), pp. 047001. doi:10.1103/PhysRevLett.112.047001

[14] H.-H. Kuo, J.-H. Chu, J.C. Palmstrom, S.A. Kivelson, and I.R. Fisher, *Ubiquitous signatures of nematic quantum criticality in optimally doped fe-based superconductors*, Science 352 (2016), pp. 958–962. doi:10.1126/science.aab0103

[15] V.K. Thorsmølle, M. Khodas, Z.P. Yin, C. Zhang, S.V. Carr, P. Dai, and G. Blumberg, *Critical quadrupole fluctuations and collective modes in iron pnictide superconductors*, Phys. Rev. B 93 (2016), pp. 054515. doi:10.1103/PhysRevB.93.054515

[16] J.C. Palmstrom, P. Walmsley, J.A.W. Straquadine, M.E. Sorensen, D.H. Burns, and I.R. Fisher, "Comparison of temperature and doping dependence of nematic susceptibility near a putative nematic quantum critical point," arXiv e-prints (2019), arXiv:1912.07574 [cond-mat.str-el]

Appendices

Appendix 1. Derivation of Equation 1

We begin with the expressions for $\tilde{\chi}''_{ab}(t)$ and $\tilde{\Lambda}_{ab}(\tau)$ in Lehmann representation:

$$\tilde{\chi}''_{ab}(t) = \frac{1}{2Z}\sum_{n,m}\Phi_{a,nm}\Phi_{b,mn}\left[e^{-\beta E_n} - e^{-\beta E_m}\right], \tag{A1}$$

$$\tilde{\Lambda}_{ab}(\tau) = \frac{1}{Z}\sum_{n,m}\Phi_{a,nm}\Phi_{b,mn}e^{-\beta E_n}e^{\tau(E_n - E_m)}. \tag{A2}$$

Fourier transform $\tilde{\chi}''(t)$ with appropriate regularisation at $t \to \pm\infty$, yielding

$$\begin{aligned}\chi''_{ab}(\omega) &= \frac{1}{2Z}\sum_{n,m}\Phi_{a,nm}\Phi_{b,mn}\left[e^{-\beta E_n} - e^{-\beta E_m}\right]e^{it(E_n - E_m)} \\ &\quad\times \frac{2\cdot 0^+}{(\omega + E_n - E_m)^2 + (0^+)^2} \\ &= \frac{1}{2Z}\sum_{n,m}\Phi_{a,nm}\Phi_{b,mn}e^{-\beta E_n}\left[1 - e^{-\beta\omega}\right] \\ &\quad\times 2\pi\delta(\omega + E_n - E_m),\end{aligned} \tag{A3}$$

with 0^+ a positive infinitesimal. We can now write $\tilde{\Lambda}_{ab}(\tau)$ in terms of $\chi''_{ab}(\omega)$

$$\begin{aligned}\tilde{\Lambda}_{ab}(\tau) &= \int\frac{d\omega}{\pi}\chi''_{ab}(\omega)\left[\frac{\exp(-\omega\tau)}{1 - e^{-\beta\omega}}\right] \\ &= \int\frac{d\omega}{2\pi}\chi''_{ab}(\omega)\left[\frac{\exp[-\omega(\tau - \beta/2)}{\sinh(\beta\omega/2)}\right],\end{aligned} \tag{A4}$$

recovering Equation (1).

Appendix 2. Example transforms

A.1. Nearly constant σ

The optical conductivity $\sigma'(\omega)$ is generically an analytic function of ω, in which case there is a formal way to express $\tilde{\Lambda}$ as follows: Starting from Equation (1) for the current-current correlator,

$$\begin{aligned}\tilde{\Lambda}(\tau) &= \int\frac{d\omega}{2\pi}\sigma'(\omega)\frac{\omega\exp[\omega(\tau - \beta/2)]}{\sinh(\beta\omega/2)} \\ &= \sigma'(\partial_\tau)\int\frac{d\omega}{2\pi}\frac{\omega\exp[\omega(\tau - \beta/2)]}{\sinh(\beta\omega/2)} \\ &= \pi T^2\ \sigma'(\partial_\tau)\ \sec^2[\pi T(\tau - \beta/2)],\end{aligned} \tag{A5}$$

where $\sigma'(\omega) = \chi''(\omega)/\omega$ is the real part of the optical conductivity, and $\sigma'(\partial_\tau)$ is obtained by expanding $\sigma'(\omega)$ in powers of ω and replacing $\omega \to \partial_\tau$. If $\sigma'(\omega)$ varies slowly as a function of

ω on the scale of T, then a low order Taylor expansion in ω is adequate. Then

$$\begin{aligned}\tilde{\Lambda}(\tau) = \pi T^2\ \sigma'(0)\ \sec^2[\pi T(\tau-\beta/2)] \times \{1 \\ + \alpha_2 \sec^2[\pi T(\tau-\beta/2)][4-2\cos[2\pi T(\tau-\beta/2)] \\ + \ldots\}\end{aligned} \tag{A6}$$

where

$$\alpha_2 = (\pi T)^2 \left[\frac{\partial_\omega^2 \sigma'}{\sigma'}\bigg|_{\omega=0} \sim \left(\frac{\pi T}{\tilde{\gamma}}\right)^2, \right. \tag{A7}$$

and we have defined $\tilde{\gamma}$ as a measure of the 'width' of the conductivity, and the expansion is reasonable so long as $\tilde{\gamma} \gg \pi T$.

A.2. Sharply peaked σ

If $\sigma'(\omega)$ is negligible except for frequencies $|\omega| \ll T$, the corresponding imaginary-time correlator is nearly constant in τ, with polynomial corrections given by moments of $\sigma'(\omega)$. This can be seen by Taylor expanding the integration kernel in the first line of Equation (A5) for $|\omega\beta|, |\omega\tau| \ll 1$:

$$\tilde{\Lambda}(\tau) = \frac{NT}{\pi}\left(1 - \frac{\gamma^2}{24T^2} + \frac{\gamma^2}{2}[\tau-\beta/2]^2 + \ldots\right), \tag{A8}$$

where the total optical weight is $N \equiv \int \sigma'(\omega)\mathrm{d}\omega$, and the squared width of the peak is $\gamma^2 = N^{-1}\int \omega^2\sigma'(\omega)\mathrm{d}\omega$.

A.3. Marginal Fermi liquid

The Raman response of many strongly correlated electron fluids can be well approximated (below a high frequency cut-off) by the 'marginal Fermi liquid' form

$$\chi''_{\mathrm{MFL}}(\omega) = A\tanh(\beta\omega/2). \tag{A9}$$

This same form arises as the local susceptibility of a two-channel Kondo impurity and in various other contexts. Transforming this expression to imaginary time yields

$$\tilde{\Lambda}(\tau) = \frac{AT}{\cos[\pi T(\beta/2-\tau)]}, \tag{A10}$$

where the divergences as $\tau \to 0$ and $\tau \to \beta$ are cut-off at short imaginary times of order the inverse cut-off.

A.4. Quantum-critical power law

Near a QCP obeying ω/T scaling, one expects order parameter correlations to have a power-law form for imaginary times τ long compared to microscopic time-scales τ_0 but short compared to the thermal time, β. To make the analysis simple, consider a pure power-law form

$$\tilde{\Lambda}(\tau) \approx C\left[\frac{1}{|\tau|^x} + \frac{1}{|\beta-\tau|^x}\right]. \tag{A11}$$

The divergences at $\tau = 0, \beta$ would be regularised at an appropriate UV cut-off scale. This can be done, e.g. by replacing $|\tau|^{-x}$ with $(\tau^2+\tau_0^2)^{-x/2}$, where $1/\tau_0$ is a high energy cutoff, and similarly for $|\beta-\tau|^{-x}$.

Working backwards, we see that for $x<2$, the corresponding expression in real-time is

$$\chi''(\omega) = \frac{C}{T^{1-x}}\, F(\beta\omega), \tag{A12}$$

where F is the scaling function

$$F(u) = \frac{\pi u}{\Gamma(x)} \left|\frac{1}{u}\right|^{2-x} \left[1 - e^{-|u|}\right], \tag{A13}$$

with the gamma function $\Gamma(x) = \int_0^\infty y^{x-1} e^{-y} dy$.

Even precisely at a QCP, one expects pure power-law behaviour of $\tilde{\Lambda}$ only for times $\tau_0 \ll \tau \ll \beta$. More generally, $\tilde{\Lambda}$ near a QCP reads

$$\tilde{\Lambda}(\tau) \approx T^x f(\tau/\beta), \tag{A14}$$

where f is a scaling function, and the scaling form holds as long as $\tau \gg \tau_0$ and $\beta - \tau \gg \tau_0$. For example, the marginal Fermi liquid form in Equation (A10) shows the same power-law behaviour for $\tau \ll \beta/2$ as does Equation (A11) with $x=1$, but differs from this expression for τ near $\beta/2$.

If $\tilde{\Lambda}(\tau)$ obeys Equation (A14) in the regime $\tau_0 \ll \tau \ll |\beta - \tau_0|$ then $\chi''(\omega)$ has the same scaling form as in Equation (A12), but the scaling function F depends on the behaviour of $\tilde{\Lambda}(\tau)$ when $\tau \sim \beta/2$. While the above expressions are pleasingly explicit, in the more general case, if ω_1 is a low frequency scale that measures the distance to the QCP (at which ω_1 would vanish), then the essential aspects of this analysis can be restated as

$$\chi''(\omega) \sim \left[\frac{\omega}{|\omega|^{2-x}}\right] \times \begin{cases} \beta|\omega| & \text{for} \quad \omega_1 \ll |\omega| \ll T \\ 1 & \text{for} \quad T \ll |\omega| \ll \tau_0^{-1} \end{cases} \tag{A15}$$

determines the frequency dependence of χ'' both in the range $T \ll \omega \ll \tau_0^{-1}$, and in the range $\omega_1 \ll \omega \ll T$, but does not by itself give the relative value of the amplitudes.